A Novel Method for the Preparation of a Highly Stable and Active CdS Photocatalyst with a Special Surface Nanostructure

Dengwei Jing and Liejin Guo*

State Key Laboratory of Multiphase Flow in Power Engineering, School of Energy and Power Engineering, Xi'an Jiaotong University, 710049 Xi'an, China

Received: February 12, 2006; In Final Form: March 30, 2006

A novel method for the preparation of a CdS photocatalyst is presented. In this method, freshly prepared CdO obtained by decomposing cadmium acetate at a certain temperature was subjected to thermal treatment in the presence of H_2S, which results in the formation of a highly stable and active CdS photocatalyst. In comparison to conventional preparation methods, CdS prepared by our method was found to be stable against both air oxidation and photocorrosion during a photocatalytic reaction. Most importantly, the special nanostep structure was observed at the surface of the sulfide photocatalyst, which was demonstrated to be crucial for the remarkable enhancement of photocatalytic hydrogen production. The apparent quantum yield at 420 nm and the energy conversion efficiency in the whole visible light region were determined to be 24.1% and 6.35%, respectively, in our experimental conditions.

1. Introduction

Conventional energy resources such as coal, petroleum products, etc., which are being used to meet most of the world's energy requirements, have been depleted to a great extent. It is therefore necessary to produce an alternative fuel that should in principle be pollution-free, storable, and economical. Hydrogen satisfies the first two conditions, and research has been focused on fulfilling the third requirement for the past few decades.[1−2] Among the various routes for hydrogen production, photocatalytic water splitting using semiconductors has received much attention, especially for its potential application on direct production of hydrogen from water utilizing solar light energy.[3−9]

Many semiconducting photocatalytic materials have been developed for hydrogen generation from water under light irradiation. Among them, CdS has been extensively studied because of its excellent properties in that the band gap (2.3 eV) corresponds well with the spectrum of sunlight and the conduction band edge is more negative than the H_2O/H_2 redox potential.[10] The common preparation technique for CdS adopted by earlier workers, as reported in the literature, is precipitation from aqueous solution of cadmium salt either by reacting with an aqueous solution of Na_2S or by bubbling H_2S gas. The precipitation frequently follows heat treatment to improve its crystallinity. However, it has been demonstrated that CdS prepared by these methods is prone to photocorrosion in the photocatalytic reaction where CdS itself is oxidized by the photogenerated holes.[11] Attempts have been made to improve the stability of the metal sulfide, for example, embedding CdS particles in a polymer matrix, coupling CdS with another wide-band-gap semiconductor, or incorporating the nanoparticles of metal sulfides into the interlayer photocatalysts.[12−15] However, few of the above-mentioned efforts have proven to be successful in terms of increasing both the stability and the efficiency of CdS. It was noted that the common feature for most of the above-mentioned CdS-based photocatalysts is that precipitation methods were selected for the preparation of CdS in these composite photocatalysts, which, in our opinion, may be the reason for their limited performance. It is assumed that a new route for the preparation of CdS with improved physicochemical properties is likely to provide an alternative solution. In this report, we present a novel method for the preparation of highly stable and photocatalytically efficient CdS with a special surface nanostructure. By comparison of the stability and the efficiency of the CdS prepared with different methods, some important factors that contribute to the high efficiency and stability of the prepared CdS photocatalysts have been investigated. The importance of this study lies in that both the preparation method and the conclusions drawn from this study might be extended to the preparation of other metal sulfide photocatalysts, which are expected to lead to the finding of photocatalysts with even higher efficiency.

2. Experimental Section

2.1. Preparation of Various CdS Samples. All chemicals were of analytical grade and used without further purification. CdS was prepared by the following three methods:

(1) CdS prepared by thermal sulfidation of the precursor:

(a) Cadmium acetate ($Cd(Ac)_2 \cdot 2H_2O$) was heated in a quartz tube at 400 °C for 2 h in flowing air to decompose acetic cadmium into CdO; (b) dry H_2S (10 mL/min) gas was then passed through the quartz tube at 200−400 °C for 4 h to sulfurize CdO into CdS; (c) after being cooled naturally to 100 °C with flowing H_2S gas, the quartz tube was allowed to cool to room temperature under N_2 atmosphere. The product was collected and then subjected to repeated washing with deionized water and then dried in a vacuum at 40 °C for 6 h. CdS prepared by this method is denoted as CdS−S or CdS−S-*m*, here *m* represents the temperature at which CdO precursor was treated with H_2S gas.

(2) CdS prepared by the precipitation method without thermal treatment:

(a) Approximately 0.1 M $Cd(Ac)_2$ and 0.1 M Na_2S were mixed in 1:1 molar ratio, followed by continuous stirring for

* Author to whom correspondence should be addressed. E-mail: lj-guo@mail.xjtu.edu.cn.

10.1021/jp060905k CCC: $33.50
Published on Web 05/23/2006

30 min at room temperature; (b) the precipitate was filtered and washed with deionized water several times and then dried in a vacuum at 40 °C for 6 h. The final product was denoted as CdS−C.

(3) CdS prepared by the precipitation method followed by thermal treatment:

(a) Approximately 0.1 M $Cd(Ac)_2$ and 0.1 M Na_2S were mixed in 1:1 molar ratio, followed by continuous stirring for 30 min at room temperature; (b) the precipitate was filtered and washed with deionized water several times; (c) the product was then subjected to high-temperature treatment at 400 or 500 °C under N_2 atmosphere for 4 h. The final product was denoted as CdS−N-*m*, where *m* represents the thermal treatment temperature.

It should be mentioned here that the two most commonly used methods for the preparation of the sulfide material were used for comparison. The difference of our method from these two methods (methods 2 and 3) is in that CdO obtained by thermolysis rather than cadmium ions was used as the cadmium source. The well-crystallized CdO precursor could thus act as a hard template to form the final CdS, which may result in the formation of some unexpected morphology and properties. In addition, all the prepared CdS samples (including Pt-loaded CdS) were stored in sealed transparent bottles placed in visible light for 7 days before being subjected to thorough characterization, in the aim of testing the stability of the prepared photocatalysts.

2.2. Characterization. The X-ray diffraction (XRD) patterns were obtained from a Rigaku D/Max-IIIA diffractometer using Cu Kα irradiation. Thermogravimetry differential thermogravimetric analysis (TG-DTA) was carried out on a Netzsch STA 449C thermal analysis instrument. The diffuse reflection of the samples was determined by a Hitachi U-4100 UV−vis−near-IR spectrophotometer. The sample morphology was observed by a JEOL JSM-6500FE scanning electron microscope. A transmission electron microscopy (TEM) study was carried on a JEOL JEM 2010 instrument. Elemental mapping over the selected regions of the photocatalytst was conducted by an energy-dispersive X-ray spectrometer (EDX) attached to the transmission electron microscope. A Raman scattering study was performed on a Jobin Yvon LabRAM HR spectrometer using 514.5 nm irradiation from an argon ion laser at 20 mW. The X-ray photoelectron spectroscopy (XPS) measurements were conducted on a PHI-550 multifunctional spectrometer. Photoluminescence (PL) spectra were recorded on a Hitachi F-3010 fluorescence spectrophotometer.

2.3. Evaluation of Photocatalytic Activity. Photocatalytic hydrogen evolution was performed in a side-irradiation Pyrex cell. The effective irradiation area for the cell is 12.56 cm^2. The reaction cell was connected to a closed gas circulation system, and the hydrogen evolved was analyzed by an on-line thermal conductivity detector (TCD) gas chromatograph (NaX zeolite column, nitrogen as a carrier gas). In all experiments, 200 mL of deionized water containing 0.2 g of catalyst and 0.25 M Na_2SO_3/0.35 M Na_2S mixed sacrificial agent was added into the reaction cell. Here, sacrificial agent was used to scavenge photogenerated holes. Nitrogen was purged through the cell before reaction to remove oxygen. The reaction solution was replaced by a fresh one every 10 h as one run to compensate for the loss of sacrificial agent, and the whole system was evacuated and purged with nitrogen after each run. Pt as a cocatalyst for the promotion of hydrogen evolution was photodeposited in situ on the photocatalyst from the precursor of $H_2PtCl_6 \cdot 6H_2O$. The temperature for all the photocatalytic reactions was kept at 35 ± 5 °C. A 300 W Xe lamp was used as the light source, and the UV part of the light was removed by a cutoff filter ($\lambda > 430$ nm, $T = 65\%$), and the irradiation power after the filter is monitored by an irradiatometer to be 70.05 mW/m^2. Apparent quantum yields defined by eq 1 were measured using a 420 nm band-pass filter and an irradiatometer. In the experiment, the irradiation power after the band-pass filter was determined to be 3.5 mW/cm^2. The energy conversion efficiency in the visible light region (using a 300 W Xe lamp combined with a 430 nm cutoff filter) was determined by eq 2

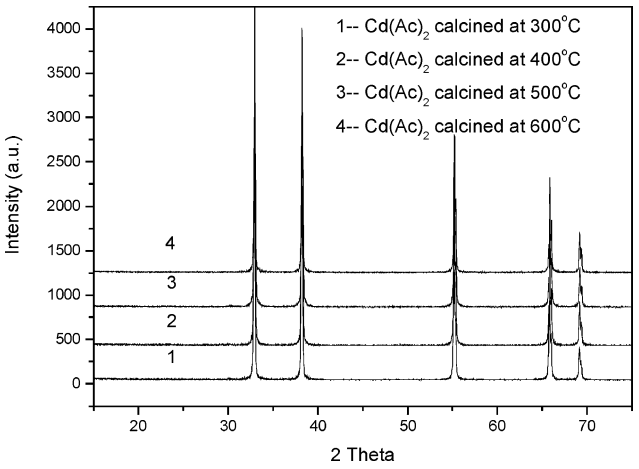

Figure 1. XRD patterns for various CdO samples obtained by calcinations of $Cd(Ac)_2$ at different temperatures for 2 h

$$\text{A.Q.Y. (\%)} = \frac{\text{number of reacted electrons}}{\text{number of incident photons}} \times 100 = \frac{\text{number of evolved } H_2 \text{ molecules} \times 2}{\text{number of incident photons}} \times 100 \quad (1)$$

$$\eta_c = \frac{\Delta G_P^0 R_P}{E_s A} \quad (2)$$

where ΔG_P^0 (J mol^{-1}) is the standard Gibbs energy for the chemical reaction forming the product(s) P, R_P (mol s^{-1}) is the rate at which the products are formed, E_s is the total incoming light irradiance (J s^{-1} m^{-2}), and A is the irradiated area.

3. Results

3.1. Crystal Structure Characterization. Figure 1 shows the XRD patterns of CdO obtained by decomposition of acetic cadmium ($Cd(Ac)_2$) at different temperatures. No noticeable difference was found for XRD patterns of the four samples. TG-DTA curves in Figure 2 reveals that the decomposition of $Cd(Ac)_2$ completed at 325 °C, where all the residual carbon species can be oxidized and removed. Therefore, in the following parts, 400 °C was chosen as the temperature for the decomposition of $Cd(Ac)_2$ to obtain CdO precursors where pure CdO can be safely obtained.

XRD patterns for various CdS−S samples are shown in Figure 3. As seen from the figure, with sulfidation temperatures of 200 and 300 °C, there remains certain amount of CdO. Complete sulfidation of the CdO precursor can be achieved at 400 °C at which no peaks attributable to CdO are found. It is noted that XRD patterns for all CdS−S samples are very sharp and exhibit only hexagonal phase CdS (Joint Committee on Powder Diffraction Standards (JCPDS) Card No. 06-0314). The intense XRD peaks of CdS−S samples indicate their good crystallinity. In contrast, XRD patterns of CdS−C (Figure 4a)

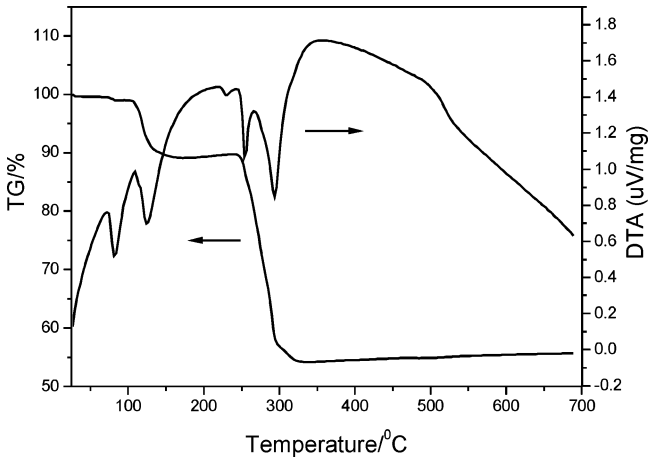

Figure 2. TG-DTA curves for $Cd(Ac)_2$

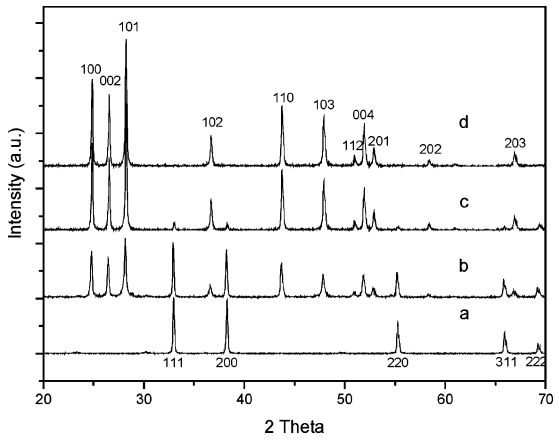

Figure 3. XRD patterns for CdO precursors treated at various temperatures in the presence of H_2S gas: (a) without treatment; (b) 200 °C; (c) 300 °C; (d) 400 °C.

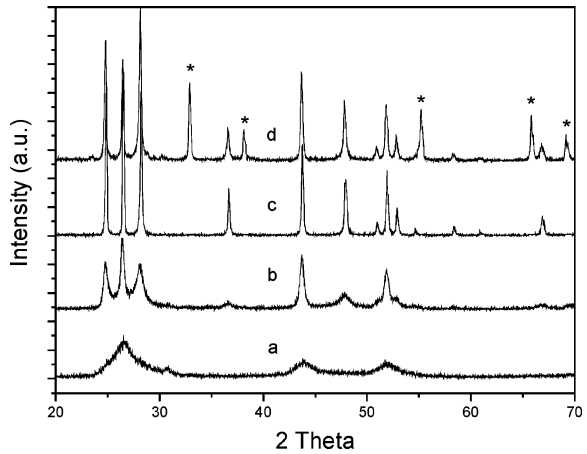

Figure 4. XRD patterns of CdS prepared by other methods: (a) CdS−C; (b) CdS−N-400; (c) CdS−N-500; (d) thermal treatment of commercial CdO at 400 °C in the presence of H_2S for 4 h

are assigned to cubic-phase CdS (JCPDS Card No. 10-0454), and the peaks are broadened due to poor crystallinity. For CdS−N-400, as shown by curve b, while some peaks indexed to hexagonal CdS appeared, its crystallinity is still poor compared to the CdS−S samples. It is also noted in curve b that some XRD peaks attributable to hexagonal phase CdS are still absent, indicating the incomplete phase evolution for CdS−N-400. Highly crystalline hexagonal CdS can be obtained with heat treatment under N_2 atmosphere as high as 500 °C (curve c). As is well-known, hexagonal phase CdS is more active than cubic-

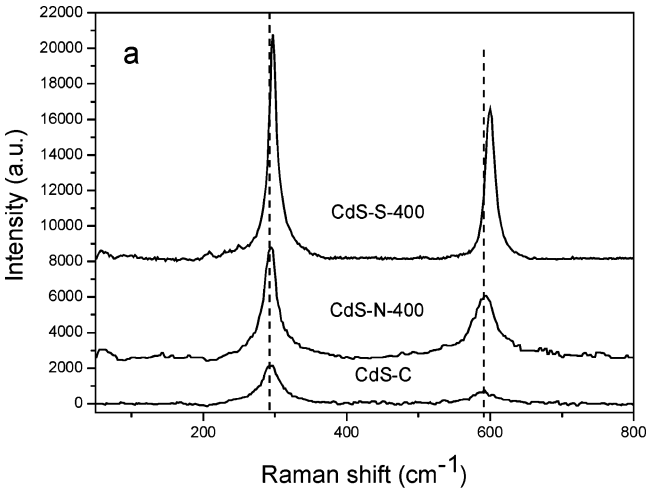

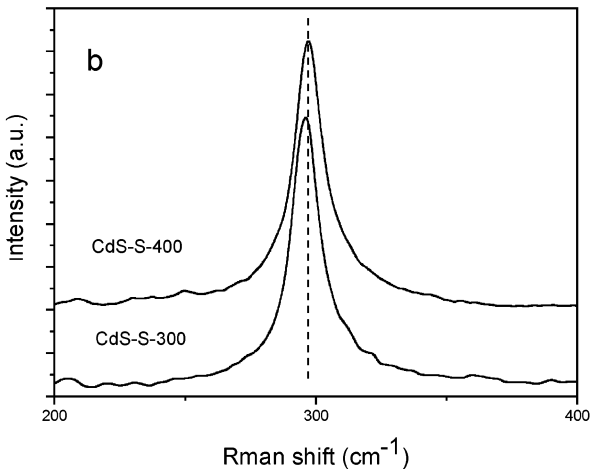

Figure 5. Raman spectra (a) for various CdS samples and (b) for CdS−S-400 and CdS−S-300

phase CdS with respect to photocatalytic hydrogen production.[2,16] However, CdS prepared by conventional precipitation methods often exhibits only the cubic phase. To promote the phase transition from cubic to more active hexagonal phase and to improve the crystallinity, thermal treatment is necessary. It is reported that phase transformation from cubic to hexagonal CdS starts at ca. 350 °C and the phase transformation is incomplete even at 400 °C.[17] In contrast, CdS prepared by our method showed good crystallinity of the hexagonal phase even under a sulfidation temperature as low as 300 °C, and no cubic-phase CdS was found at all sulfidation temperatures.

A Raman spectrum is a useful tool for the investigation of the microstructure of crystalline materials. Figure 5a shows the micro-Raman spectra of various CdS samples at room temperature. The Raman peaks around 300 cm^{-1} are attributed to a CdS-like longitudinal optical mode (1LO) resulting from the A1 mode of the Cd−S bond vibration.[18] The first overtone of the A1 mode is located at ca. 600 cm^{-1}(2LO). It can be seen from Figure 5a that the 1LO-to-2LO ratio increased in the order of CdS−C < CdS−N-400 < CdS−S-400. The higher ratio indicates the increased crystalline size of CdS.[19] A blue shift of the Raman modes for CdS−S-400 compared with the other two CdS samples was observed, as indicated by dotted lines in Figure 5a. It is reported that the 1LO mode for single-crystal CdS is centered at 305 nm.[20] A smaller frequency shift of the 1LO mode for CdS−S from single-crystal CdS implies its better microstructure. The above results suggest that CdS prepared by our method is more ordered not only in the long range (as

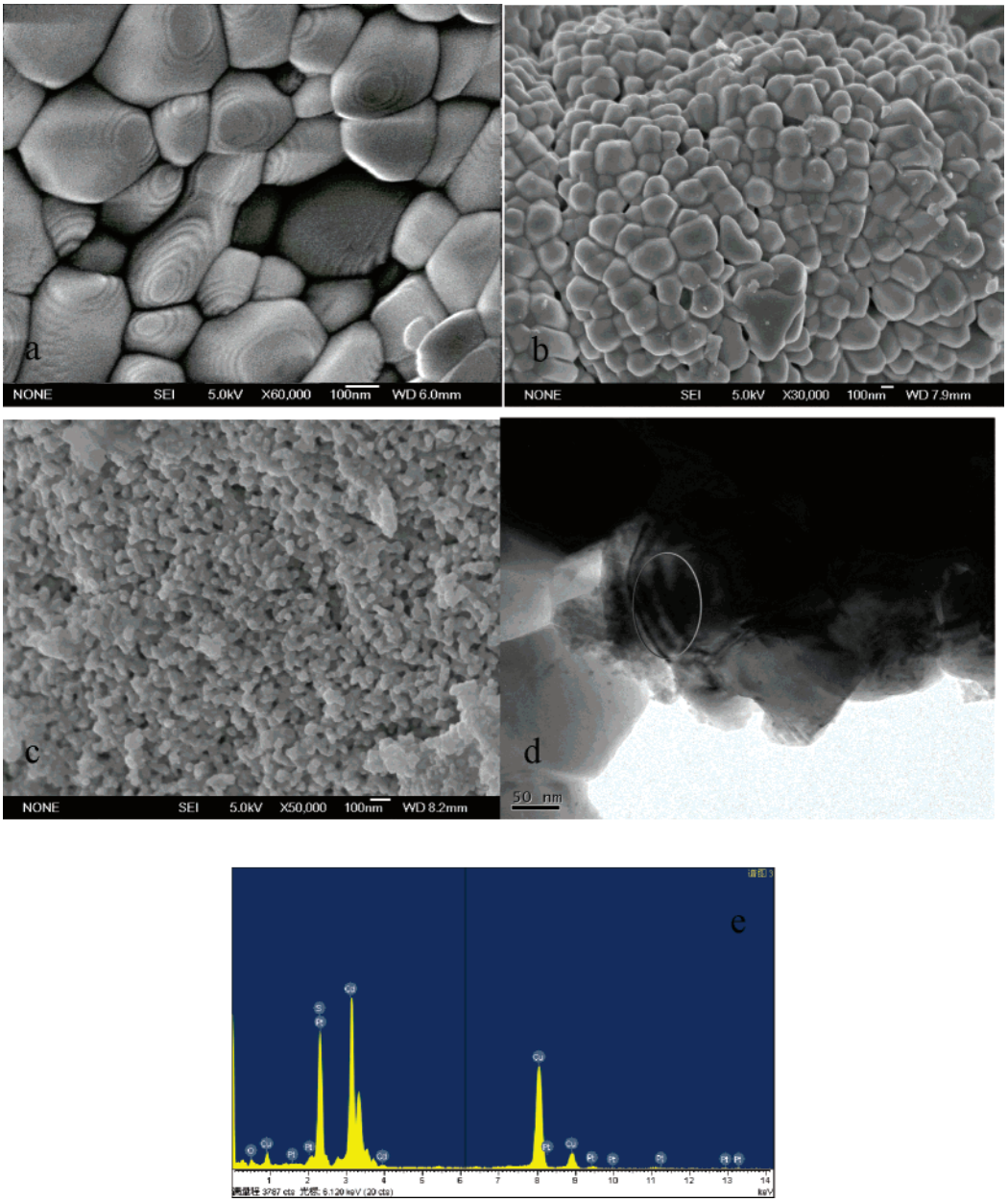

Figure 6. SEM images of (a) CdS−S-400, (b) CdO obtained by thermal treatment of $Cd(Ac)_2$ at 400 °C for 2 h, and (c) CdS−N-400, (d) TEM image of 2 wt % Pt-loaded CdS−S-400, and (e) microarea EDX analysis along the nanostep within the circular area in (d).

determined by XRD) but also in the short range (as revealed by the Raman spectrum). LO modes of CdS−S-400 and CdS−S-300 are shown in Figure 5b. It can be seen that the peak positions for the two samples are also different, although their peak intensities are comparable. Similar peak intensities indicate their similar crystallinity, as also confirmed by XRD results. We thus ascribe the difference of peak positions for the two samples to the existence of oxygen atoms in the bulk of CdS−S-300, considering that the vibration frequency of the Cd−O bond should be smaller than that of the Cd−S bond.[21]

3.2. Surface Morphology. Figure 6a shows a typical scanning electron microscopy (SEM) image of CdS−S-400; close-packed round particles of 100−300 nm sizes are observed. It is worth noting that screw-thread-like nanostep structures exist at the surface of many particles. As shown in Figure 6b, the SEM image for CdO also shows round particles of 100−300 nm. However, its surface is smooth, and no any surface patterns can be observed. We can thus conclude that the special surface morphology for CdS−S-400 is formed during the sulfidation process in the presence of H_2S. However, CdS−N-400 exhibited aggregation of CdS primary nanoparticles of 20−30 nm in size with rough surfaces, as shown in Figure 6c. A TEM image of 2 wt % Pt-loaded CdS−S-400 was also recorded. As in Figure 6d, we can also see the existence of the nanostep structure. However, Pt clusters could not be observed. Further selected-area EDX analysis along the nanostep of the CdS−S-400 surface (Figure 6d, marked by a circle) reveals the considerable enrichment of Pt at the nanostep area compared to that of other places. As shown by Figure 6e, the weight percent of Pt within the circle area of Figure 6d is determined to be 4.1%, much higher than the nominal Pt loading value of 2%. Therefore, it can be inferred that the photodeposited Pt clusters might exist in the form of ultrafine particles with sizes well bellow the detection limit of the TEM instrument and these Pt particles may preferably exist at nanostep areas.

3.3. Compositional Analysis in the Bulk and at the Surface. X-ray photoelectron spectroscopy analysis was carried out on three CdS samples. As shown in Figure 7, only peaks

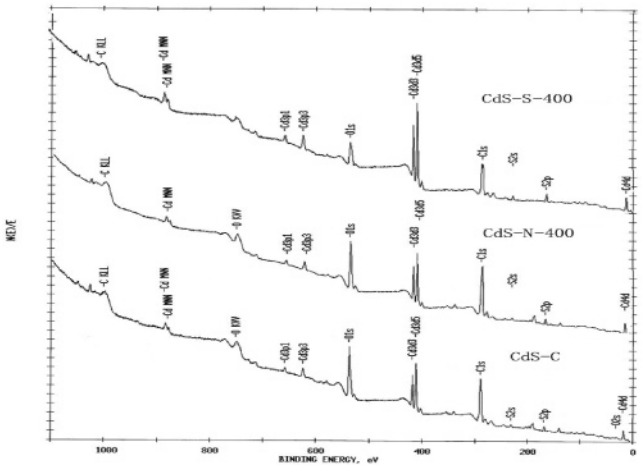

Figure 7. XPS results for various CdS samples.

TABLE 1: Elemental Analysis of Various CdS Samples

samples	Cd/S atomic ratio[a]	surface oxygen content wt %[a]	bulk oxygen content wt %[b]
CdS−S-300	1.117	8.4%	6.5%
CdS−S-400	1.073	2.1%	0.6%
CdS−C	1.107	6.9%	2.4%
CdS−N-400	1.114	7.2%	2.7%

[a] Estimated from the XPS peak areas. [b] Obtained from EDX measurements. Here the elemental analysis results were taken as the bulk composition.

assigned to Cd, S, O, and C electrons were identified for all the samples. Here, C peaks may originate from absorbed gaseous molecules. Attention was paid to the significant difference of the O 1s peak around 531 eV for these samples. It can be seen that CdS−S-400 has the smallest O 1s peak compared to CdS−N-400 and CdS−C. By estimation of the peak areas of selected XPS peaks, surface elemental analysis was conducted, and the results are summarized in Table 1. The Cd/S atomic ratios at the surfaces were determined to be 1.073, 1.107, and 1.114 for CdS−S-400, CdS−C, and CdS−N-400, respectively.

Elemental analysis for various CdS samples was also conducted by the EDX instrument attached to the transmission electron microscope. The results are also given in Table 1. Note that the elemental analysis results obtained by EDX are considered here as the bulk composition of the photocatalysts, with the consideration that the analysis depth of EDX is much deeper than that of XPS.[22] As shown in Table 1, more or less amounts of oxygen can be found in all the samples. Since the samples have been subjected to high vacuum treatment before TEM analysis, oxygen atoms attributable to absorbed molecules could be safely excluded. It is also noted that the oxygen contents obtained by EDX are much smaller than the surface oxygen contents estimated by XPS for all the samples except for CdS−S-300 that contains a certain amount of CdO. It is thus unlikely that the much higher oxygen content obtained by XPS is purely due to absorbed impurities. One can thus infer that most of the oxygen existed near the surface for CdS−S-400, CdS−C, and CdS−N-400. The existence of oxygen atoms could be attributed to partial oxidation of the CdS surface during exposure in air, as reported by the literature.[23] The above elemental analysis results implied that CdS−S-400 is most stable against surface oxidation. However, CdS−N-400, although with improved crystallinity compared to CdS−C, is most susceptible to oxidation in air.

3.4. Photophysical Properties. Figure 8 shows the UV−vis absorption spectra for various CdS samples. It is seen from the

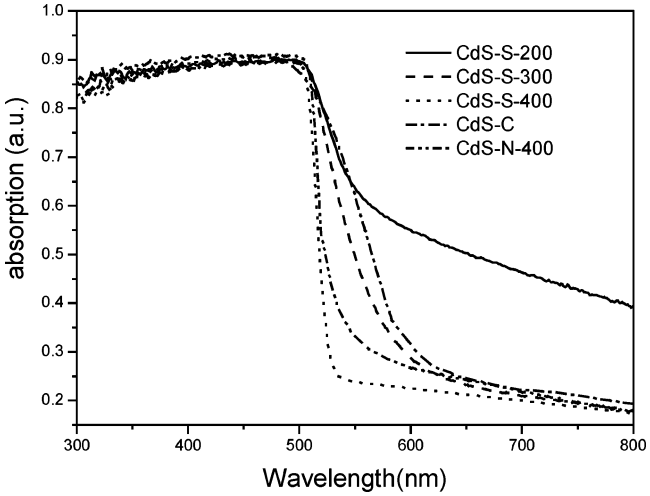

Figure 8. Diffuse reflectance spectra for various CdS samples.

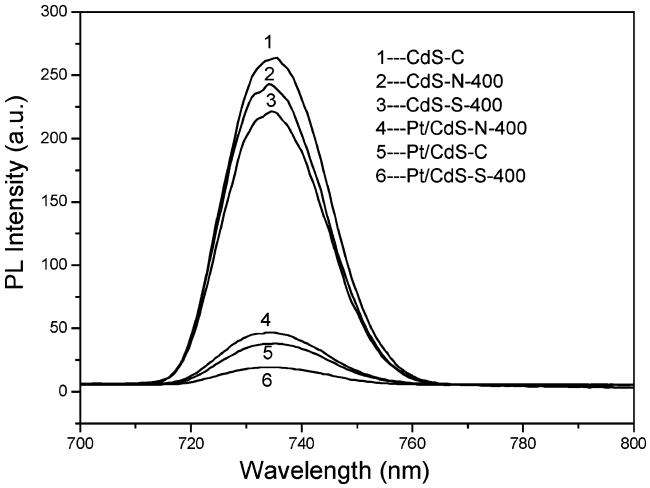

Figure 9. PL spectra for various CdS samples before and after 2 wt % Pt loading, excitation 370 nm.

figure that, besides the main absorption between 500 and 600 nm, CdS−S-200 shows a broad absorption throughout the visible light region. With the increase of treatment temperature in the presence of H_2S to 400 °C, the absorption after 600 nm almost disappeared. The sharp absorption curve with an onset around 520 nm indicates the absence of absorption due to impurity energy levels and almost purely resulted from the band-gap transition of electrons from the valance band to the conduction band of CdS. The band gap of CdS−S-400 is estimated to be 2.38 eV from the onset of absorption, in agreement with the reported value for CdS semiconductors.[24] In contrast, both CdS−C and CdS−N-400 have prominent absorption in the visible light region longer than 600 nm.

Photoluminescence spectra on the prepared CdS samples before and after the loading of Pt were recorded. As shown in Figure 9, an intense emission peak centered at ca. 734 nm can be observed for all the CdS samples, and the PL peak intensities increase in the order of CdS−S-400 < CdS−N-400 < Cd−C. As has been reported, the peak at 734 nm can be related to electron−hole recombination processes within the semiconductor.[25] It is thus inferred that the CdS prepared by our method has the least lattice defects, which, in turn, result in less electron−hole recombination. The PL spectra of various CdS samples after Pt loading are also shown in Figure 9. Considerable fluorescence quenching is observed. The quenching of fluorescence indicates transfer of photogenerated electrons from the semiconductor to the Pt metal.[26−27] Again, CdS−S-400

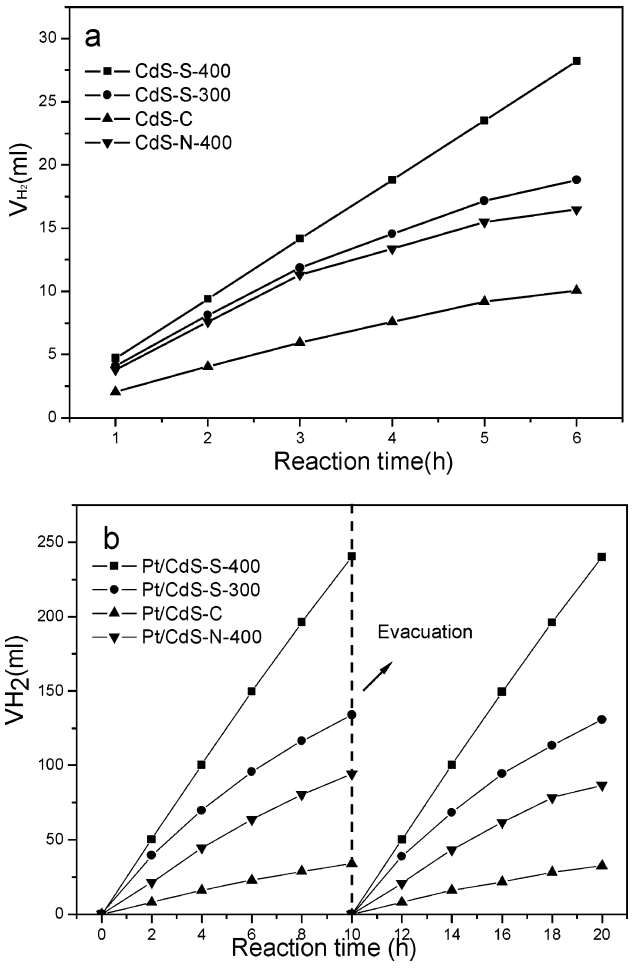

Figure 10. Amount of H_2 evolved vs irradiation time on various CdS samples under the visible part of Xe lamp irradiation (300 W, $\lambda > 430$ nm, $T = 65\%$) in a mixed 0.25 M Na_2SO_3/0.35 M Na_2S solution with 0.2 g of catalyst: (a) without Pt loading; (b) with 2 wt % Pt loading.

shows the most intense fluorescence quenching after Pt loading compared to other samples, indicative of the more favorable contacts between Pt and this CdS sample. It is worth noting that Pt-loaded CdS−N-400 has a higher fluorescence emission than Pt-loaded CdS−C. As has been determined by elemental analysis, CdS−N-400 is the most susceptible to surface oxidation. It seems that the existence of oxygen on the surface of CdS is detrimental to the close contact between Pt and CdS.

3.5. Photocatalytic Activity Evaluation. Photocatalytic H_2 productions with various photocatalysts were evaluated. Control experiments showed no appreciable H_2 evolution in the absence of either irradiation or photocatalyst. As shown in Figure 10a, CdS−S-400 exhibits the highest activity toward photocatalytic hydrogen production. The linear relationship between hydrogen evolution and time indicates its good stability against photocorrosion. For CdS−N-400 and CdS−C, however, the hydrogen evolution rates were lower and showed a slight decrease after photocatalytic reaction for 6 h. The photocatalytic activity of CdS−S-300 also showed a slight decrease after reaction for 6 h, indicting that the existence of oxygen atoms in the bulk may be one reason responsible for CdS photocorrosion.

To improve the photocatalytic hydrogen evolution, Pt as a cocatalyst should be loaded on the photocatalyst to provide active sites for hydrogen production.[28−30] Photocatalytic hydrogen production over various Pt-loaded CdS photocatalysts is given in Figure 10b. As shown in the figure, all CdS samples showed enhanced hydrogen production after loading Pt. In particular, Pt-loaded CdS−S-400 shows a 5-fold increase of hydrogen production, and the hydrogen evolution rate amounts to 25.2 mL/h. Its quantum yield at 420 nm was determined to be 24.1% according to eq 1, and the energy conversion efficiency in the whole visible light region was calculated by eq 2 to be 6.35%. In contrast, the quantum yields of Pt-loaded CdS−N-400 are only 11.7% in our experimental conditions. The activity of Pt-loaded CdS−S-300, which also had a similar surface nanostructure as observed by SEM (data not shown), was investigated. While it underwent a rapid decrease of photocatalytic activity after reaction for several hours, the photocatalyst showed a high initial hydrogen evolution rate of 19.7 mL/h, which again implies the importance of the special surface nanostructure for the high photocaatlytic activity. By comparison of the initial hydrogen evolution rate after five runs of the photocatalytic reaction with that of the first run, the deactivation owning to photocorrosion for various Pt-loaded CdS samples were evaluated. The photocorrosion extent increased in the order of CdS−S-400 < CdS−C < CdS−S-300 < CdS−N-400. It can be concluded that the existence of oxygen atoms at the surface and/or in the structure of CdS would accelerate the photocorrosion process of the sulfide photocatalyst.

4. Discussion

Conventionally, CdS can be prepared by a precipitation method that often gives rise to the formation of less active cubic CdS with poor crystallinity. While thermal treatment could improve its crystallinity and promote phase transformation, high temperature as high as 500 °C is often needed to obtain highly crystalline CdS (Figure 4). Furthermore, as shown by our results, thermal treatment on precipitated CdS would make it more susceptible to surface oxidation and hence increased photocorrosion. Our results showed that the normal thermal process required for CdS crystallization could be changed by sulfurizing CdO into the final product. As shown by Figure 1, highly crystalline CdO can be obtained at a temperature around 300 °C by decomposing cadmium acetate. Sulfidation of CdO by H_2S at as low as 300 °C will result in the formation of highly crystalline hexagonal phase CdS (Figure 3), and pure CdS can be obtained at a sulfidation temperature of 400 °C. By such a route, the crystallization and phase transformation temperatures of CdS can be significantly lowered compared to the above-mentioned conventional thermal treatment method for the preparation of CdS.

It is interesting to find that the surface nanostructures exist at the surfaces of most CdS−S samples (Figure 6). The nanostep was found to be formed during the sulfidation process. In fact, a similar nanostructure has also been observed by Kudo et al. for another sulfide photocatalyst.[31] However, to the best of our knowledge, no such nanostructure has been reported for CdS. While their underlying formation mechanism might be different, the importance of the nanostep surface to the great enhancement of photocatalytic reaction has been well demonstrated by previous results, especially for photocatalytic hydrogen production from water.[31−32] Our data further supported this demonstration. Although direct observation of Pt clusters failed, the considerable enrichment of Pt clusters within a nanostep area and the resultant high photoactivity for hydrogen production indeed indicated the importance of such structures for the favorable interaction between Pt and the CdS surface. Further, the preferential deposition of Pt implied that photogenerated electrons could readily migrate to the surface nanostep area, where the H_2PtCl_6 precursor was reduced to metallic Pt by the electrons.

By comparison of the UV−vis spectra and photocatalytic hydrogen production results (Figures 8 and 10), it is found that there is no necessary correlation between visible light adsorption and the photoactivity in visible light. As shown in Figure 8, both CdS−C and Cd−N samples show stronger visible light adsorption than CdS−S-400. However, the hydrogen production showed a reverse trend with respect to the light absorption ability for three CdS samples. It can be inferred that photoabsorption from shallow impurity energy levels, as for the CdS−C and CdS−N-400 cases, would not contribute to the hydrogen production and would even be detrimental in view of effective photoutilization. On the contrary, it is found that PL spectra can be a reliable tool for the prediction of hydrogen production activity of photocatalysts. CdS with weak fluorescence at 734 nm means less recombination of electrons and holes, thereby higher activity. The PL results also showed that oxygen atoms existing at the surfaces of CdS are unfavorable for close contact between Pt and CdS, which results in a lowered efficiency of electron transfer from semiconductor to Pt. Thus it is suggested that to obtain an efficient Pt-loaded CdS photocatalyst the sulfide itself should be stable against air oxidation.

Our photocatalytic hydrogen production results suggested that photogenerated electrons with enough negative potential, good crystallinity, and fewer crystal defects are indispensable for efficient hydrogen production and the special surface morphology sometimes indeed makes a great contribution. These conclusions are different from most of cases for photocatalytic degradation of organic compounds where photogenerated holes are often utilized either directly or indirectly for its oxidizing power.[33] In fact, there are many examples of intentional generation of vacancy and defects in photocatalysts to improve their activity with respect to the photocatalytic degradation of organics.[34]

Additionally, the steady hydrogen production activity for the Pt-loaded CdS−S-400 sample compared with that of CdS−S-300 suggests that the existence of oxygen ions is detrimental for such a sulfide photocatalyst and would accelerate the photocorrosion process. This again demonstrated that a sulfide photocatalyst with fair stability in air is essential for its anti-photocorrosion ability.

5. Conclusion

In summary, a new method for the preparation of highly stable and active CdS was presented. The prepared CdS−S showed enhanced stability against both air oxidation and photocorrosion and extremely high photocatalytic activity toward hydrogen production compared to CdS samples prepared by two conventional methods. By this route, the normal thermal process required for CdS crystallization is avoided, and we can obtain hexagonal CdS of better crystallinity under lower temperatures. The special surface nanostructure for CdS−S samples formed during the sulfidation process was found, and it was demonstrated that the existence of such a nanostructure is crucial for the remarkable enhancement of hydrogen production after loading Pt. It was also proved that the existence of oxygen at the surface and/or in the structure of CdS was detrimental and would accelerate photocorrosion of the sulfide photocatalyst. Furthermore, we have found that our method of preparing CdS could be extended to the preparation of other binary and ternary metal sulfides such as ZnS and $Cd_xZn_{1-x}S$. Significant improvement of the stability and activity of the photocatalysts was also found, and the results will be reported elsewhere. We have also loaded CdS prepared by our method on certain substrates of high surface area, and results of interest were found too. It should however be mentioned that freshly decomposed CdO is important for our method. As mentioned in this paper, sulfidation of commercial CdO is much more difficult than freshly decomposed CdO, the reason for which is currently under investigation in our lab.

Acknowledgment. The authors gratefully acknowledge the financial support of the National Natural Science Foundation of China (Grant No. 50521604) and the National Basic Research Program of China (Grant No. 2003CB214500).

References and Notes

(1) Hao, X. H.; Guo, L. J.; Mao, X.; Zhang, X. M.; Chen, X. J. *Int. J. Hydrogen Energy* **2003**, *28*, 55.

(2) Ashokkumar, M. *Int. J. Hydrogen Energy* **1998**, *23*, 427.

(3) Domen, K.; Kudo, A.; Ohnishi, T. *J. Catal.* **1986**, *102*, 92.

(4) Zou, Z.; Ye, J.; Sayama, K.; Arakawa, H. *Nature* **2001**, *414*, 625.

(5) Zou, Z.; Ye, J.; Arakawa, H. *J. Phys. Chem. B* **2002**, *106*, 517.

(6) Hitoki, G.; Takata, T.; Kondo, J. N.; Hara, M.; Kobayashi, H.; Domen, K. *Chem. Commun.* **2002**, 1698.

(7) Jing, D. W.; Zhang, Y. J.; Guo, L. J. *Chem. Phys. Lett.* **2005**, *415*, 74.

(8) Liu, M. Y.; You, W. S.; Lei, Z. B.; Zhou, G.H.; Yang, J. J.; Wu, G. P.; Ma, G. J.; Luan, G. Y. Takata, T.; Hara, M.; Domen, K.; Li, C. *Chem. Commun.* **2004**, 2193.

(9) Kato, H.; Asakura, K.; Kudo, A. *J. Am. Chem. Soc.* **2003**, *125*, 3082.

(10) Matsumura, M.; Saho, Y.; Tsubomura, H. *J. Phys. Chem.* **1983**, *87*, 3807.

(11) Meissner, D.; Memming, R.; Kastening, B. *J. Phys. Chem.* **1988**, *92*, 3476−3483.

(12) Mau. A.; Huang, C. B.; Kakuta, N.; Bard, A.J.; Campion, A.; Fox, M. A.; White, J. M.; Webber, S. E. *J. Am. Chem. Soc.* **1984**, *106*, 6537.

(13) Fujii, H.; Ohtaki, M.; Eguchi, K. *J. Mol. Catal. A: Chem.* **1998**, *129*, 61.

(14) Guan, G. Q.; Kida, T.; Kusakabe, K.; Kimura, K.; Fang, X. M.; Ma, T. L.; Abe, E.; Yoshida, A. *Chem. Phys. Lett.* **2004**, *385*, 319.

(15) Shangguan, W.; Yoshida, A. *J. Phys. Chem. B* **2002**, *106*, 12227.

(16) Sahu, H.; Arora, M. K.; Upadhyay, S. N.; Sinha, A. S. K. *Ind. Eng. Chem. Res.* **1998**, *37*, 4682.

(17) Gorer, S.; Hodes, G.; Sorek, Y.; Reisfeld. R. *Mater. Lett.* **1997**, *31*, 209−214.

(18) Liang, Y. Q.; Zhai, L.; Zhao, X. S.; Xu, D. S. *J. Phys. Chem. B* **2005**, *109*, 7120.

(19) Shiang, J. J.; Risbud, S. H.; Alivisatos, A. P. *J. Chem. Phys.* **1993**, *98*, 8432.

(20) Leite, R. C. C.; Porto, S. P. S. *Phys. Rev.* **1966**, *17*, 10.

(21) Narayanan, K. L.; Vijayakumar, K. P.; Nair , K. G. M.;, Undarakkannan, B.; Kesavamoorthy, R. *Nucl. Instrum. Methods Phys. Res., Sect. B* **2000**, *160*, 471.

(22) Maeda, K.; Teramura, K.; Takata, T.; Hara, M.; Saito, N.; Toda, K.; Inoue, Y. Kobayashi, H.; Domen, K**.** *J. Phys. Chem. B* **2005**, *109*, 20504.

(23) Mills, A., Williams, G. *J. Chem. Soc., Faraday Trans.* 1989, 85, 503.

(24) Gao, J.; Sun, J. Z.; Hong, J.; Li, H. Y.; Chen, H. Z.; Wang, M. *Adv. Mater.* **2004**, *16*, 84.

(25) Shangguan, W. F.; Yoshida, A. *J. Phys. Chem. B* **2002**, *106*, 12227.

(26) Bühler, N.; Meier, K.; Reber, J. *J. Phys. Chem.* **1984**, *88*, 3261.

(27) Hirai, T.; Suzuki, K.; Komasawa, I. *J. Colloid Interface Sci.* **2001**, *244*, 262.

(28) Zou, Z.; Arakawa, H. *J. Photochem. Photobiol., A* **2003**, *158*, 145.

(29) Li, Y. X.; Lu, G. X.; Li, S. B. *J. Photochem. Photobiol., A* **2002**, *152*, 219.

(30) Li, Y. X.; Lu, G. X.; Li, S. B. *Appl. Catal., A* **2001**, *214*, 179.

(31) Tsuji, I.; Kato, H.; Kobayashi, H.; Kudo, A. *J. Am. Chem. Soc.* **2004**, *126*, 13406.

(32) Zou, Z.; Ye, J. H.; Arakawa, H. *J. Phys. Chem. B* **2002**, *106*, 13098.

(33) Hoffmann, M. R.; Martin, S. T.; Choi, W.; Bahnemannt, D. W. *Chem. Rev.* **1995**, *95*, 69−96.

(34) Hong, X. T.; Wang, Z. P.; Cai, W. M.; Lu, F.; Zhang, J.; Yang, Y. Z.; Ma, N.; Liu, Y. J. *Chem. Mater.* **2005**, *17*, 1548.